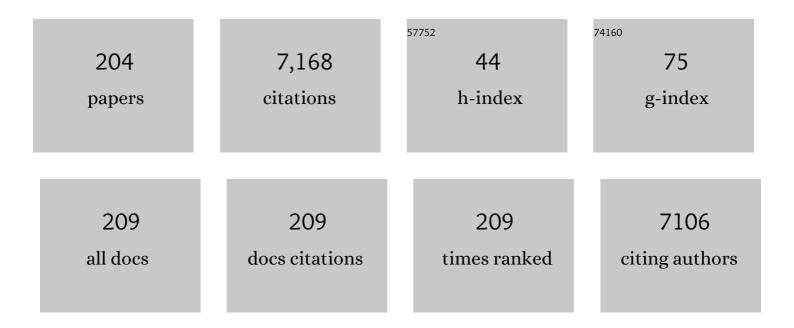
George P Demopoulos

List of Publications by Year in descending order

Source: https://exaly.com/author-pdf/1491215/publications.pdf Version: 2024-02-01



#	Article	IF	CITATIONS
1	Silicon doped carbon nanotubes as high energy anode for lithium-ion batteries. Materials Today Communications, 2022, 30, 103158.	1.9	8
2	Selenate Se(VI) reduction to elemental selenium on heterojunctioned rutile/brookite nano-photocatalysts with enhanced charge utilization. Chemical Engineering Journal, 2022, 437, 135470.	12.7	5
3	Graphene nanobuds as a novel anode design paradigm with superior Li-ion storage capacity and rate capability. Carbon, 2022, 199, 486-496.	10.3	3
4	Defect Engineering of Iron-Rich Orthosilicate Cathode Materials with Enhanced Lithium-Ion Intercalation Capacity and Kinetics. ACS Applied Energy Materials, 2020, 3, 675-686.	5.1	3
5	Electrophoretically co-deposited Li4Ti5O12/reduced graphene oxide nanolayered composites for high-performance battery application. Energy Storage Materials, 2020, 26, 560-569.	18.0	33
6	Nanoscale assembling of graphene oxide with electrophoretic deposition leads to superior percolation network in Li-ion electrodes: TiNb2O7/rGO composite anodes. Nanoscale, 2020, 12, 23092-23104.	5.6	14
7	A sustainable light-chargeable two-electrode energy storage system based on aqueous sodium-ion photo-intercalation. Sustainable Energy and Fuels, 2020, 4, 4789-4799.	4.9	11
8	Core hole screened electron energy loss calculations of beam damaged lithium fluoride. Ultramicroscopy, 2020, 219, 113126.	1.9	0
9	Silicate Nanocrystals: PEDOT Encapsulated and Mechanochemically Engineered Silicate Nanocrystals for High Energy Density Cathodes (Adv. Mater. Interfaces 13/2020). Advanced Materials Interfaces, 2020, 7, 2070075.	3.7	0
10	Toward an Allâ€Ceramic Cathode–Electrolyte Interface with Lowâ€Temperature Pressed NASICON Li _{1.5} Al _{0.5} Ge _{1.5} (PO ₄) ₃ Electrolyte. Advanced Materials Interfaces, 2020, 7, 2000164.	3.7	17
11	PEDOT Encapsulated and Mechanochemically Engineered Silicate Nanocrystals for High Energy Density Cathodes. Advanced Materials Interfaces, 2020, 7, 2000226.	3.7	4
12	Hot Press Method: Toward an Allâ€Ceramic Cathode–Electrolyte Interface with Lowâ€Temperature Pressed NASICON Li _{1.5} Al _{0.5} Ge _{1.5} (PO ₄) ₃ Electrolyte (Adv. Mater. Interfaces 12/2020). Advanced Materials Interfaces, 2020, 7, 2070069.	3.7	1
13	Unusual Li-ion Intercalation Activation with Progressive Capacity Increase in Orthosilicate Nanocomposite Cathode. Journal of Physical Chemistry C, 2020, 124, 5966-5977.	3.1	3
14	Progress and Status of Hydrometallurgical and Direct Recycling of Li-Ion Batteries and Beyond. Materials, 2020, 13, 801.	2.9	205
15	Tunable Composition Aqueous-Synthesized Mixed-Phase TiO2 Nanocrystals for Photo-Assisted Water Decontamination: Comparison of Anatase, Brookite and Rutile Photocatalysts. Catalysts, 2020, 10, 407.	3.5	41
16	Electrochemical Re-Functionalization of Spent FePO4 Originating from LiFePO4 Battery Recycling. ECS Meeting Abstracts, 2020, MA2020-01, 81-81.	0.0	0
17	Effect of the Electron Transport Layer on the Photovoltaic Properties of Hybrid Organic Inorganic Perovskites Solar Cells: Cross-Section of Optics, Morphology, Composition and Quality. ECS Meeting Abstracts, 2020, MA2020-01, 872-872.	0.0	0
18	Enhanced Capacity and Retention in Lithium Iron Orthosilicate Cathode Via Tuning Its Composition By Hydrothermal Synthesis. ECS Meeting Abstracts, 2020, MA2020-01, 153-153.	0.0	0

#	Article	IF	CITATIONS
19	Improving 2D Hybrid Energy Storage Electrode Homogeneity Via Graphene Oxide/Active Nanomaterial Electrophoretic Co-Deposition. ECS Meeting Abstracts, 2020, MA2020-01, 597-597.	0.0	Ο
20	Mechanochemical Engineering of Polymer-Coated Silicate Nanocrystal Cathodes. ECS Meeting Abstracts, 2020, MA2020-01, 388-388.	0.0	0
21	Synthesis of Mixed Phase nanoTiO2 particles & Their Application in Photocatalytic Water Decontamination. ECS Meeting Abstracts, 2020, MA2020-01, 2928-2928.	0.0	0
22	(Invited) Composition and Interfacial Engineering of Lithium Iron Orthosilicate Cathodes with Superior Intercalation Properties. ECS Meeting Abstracts, 2020, MA2020-02, 41-41.	0.0	0
23	New Insight into Sulfurized and Selenized Kesterite–Titania Nanostructures for CdS-free and HTM-free Photovoltaic and Voltage-Modulated Photodetecting Applications. ACS Sustainable Chemistry and Engineering, 2019, 7, 15093-15101.	6.7	6
24	Aqueous-based Binary Sulfide Nanoparticle Inks for Cu2ZnSnS4 Thin Films Stabilized with Tin(IV) Chalcogenide Complexes. Nanomaterials, 2019, 9, 1382.	4.1	4
25	Kinetics of iron(III)-catalyzed oxidation of arsenic(III) in acidic solutions with SO2/O2 gas mixture using different iron sources. Hydrometallurgy, 2019, 189, 105130.	4.3	7
26	Mechanochemically tuned structural annealing: a new pathway to enhancing Li-ion intercalation activity in nanosized l² _{II} Li ₂ FeSiO ₄ . Journal of Materials Chemistry A, 2019, 7, 13705-13713.	10.3	6
27	Lithium Photoâ€intercalation of CdSâ€Sensitized WO ₃ Anode for Energy Storage and Photoelectrochromic Applications. ChemSusChem, 2019, 12, 2220-2230.	6.8	36
28	Unveiling the mechanism of improved capacity retention in <i>Pmn</i> 2 ₁ Li ₂ FeSiO ₄ cathode by cobalt substitution. Journal of Materials Chemistry A, 2019, 7, 25399-25414.	10.3	11
29	Highly conductive NMP-free carbon-coated nano-lithium titanate/carbon composite electrodes via SBR-assisted electrophoretic deposition. Electrochimica Acta, 2019, 299, 107-115.	5.2	22
30	Hydrothermal crystallization of Pmn21 Li2FeSiO4 hollow mesocrystals for Li-ion cathode application. Chemical Engineering Journal, 2019, 359, 1592-1602.	12.7	26
31	Ethylenediamine-Enabled Sustainable Synthesis of Mesoporous Nanostructured Li2FellSiO4 Particles from Fe(III) Aqueous Solution for Li-Ion Battery Application. ACS Sustainable Chemistry and Engineering, 2018, 6, 7458-7467.	6.7	14
32	Phase Transition of FeSO4·7H2O to FeSO4·H2O in the H2SO4–HCl–H2O System by Modeling Solubility. ACS Sustainable Chemistry and Engineering, 2018, 6, 2207-2219.	6.7	4
33	Development of an Encapsulation Process to Extend the Stability of Scorodite Under Wider pH and Redox Potential Range Conditions. Minerals, Metals and Materials Series, 2018, , 1411-1420.	0.4	4
34	Hydrothermal Production of Lithium Metal Silicate Powders with Controlled Properties for Application to Li-ion Batteries. Minerals, Metals and Materials Series, 2018, , 2555-2563.	0.4	0
35	Nanoengineering of the Cu ₂ ZnSnS ₄ –TiO ₂ interface <i>via</i> atomic layer deposition of Al ₂ O ₃ for high sensitivity photodetectors and solid state solar cells. Journal of Materials Chemistry A, 2018, 6, 11507-11520.	10.3	27
36	Hydrolytic Precipitation of Nanosized TiO2 Phases for Use as Photocatalytic Sorption Media in Effluent Treatment. Minerals, Metals and Materials Series, 2018, , 1809-1818.	0.4	0

#	Article	IF	CITATIONS
37	Lithium-doped Cu2ZnSnS4 superstrate solar cells with 5% efficiency – An alternative to thin film kesterite photovoltaics. Nano Energy, 2018, 53, 130-134.	16.0	26
38	In Situ TEM Investigation of Electron Irradiation Induced Metastable States in Lithium-Ion Battery Cathodes: Li ₂ FeSiO ₄ versus LiFePO ₄ . ACS Applied Energy Materials, 2018, 1, 3180-3189.	5.1	20
39	Characterization of Lithium in Batteries with EDS and EELS. ECS Meeting Abstracts, 2018, , .	0.0	0
40	In Situ Conductive Coating Strategies for Nanocrystal-Based Li-Ion Battery Electrodes Beyond Carbonization. ECS Meeting Abstracts, 2018, , .	0.0	0
41	Application of Carbon Nanotubes Doped with Silicon As the Anode Electrode for Lithium Ion Battery. ECS Meeting Abstracts, 2018, , .	0.0	0
42	Annealing-regulated elimination of residual strain-induced structural relaxation for stable high-power Li4Ti5O12 nanosheet anodes. Nano Energy, 2017, 32, 533-541.	16.0	29
43	Removal of antimony from concentrated solutions with focus on tripuhyite (FeSbO4) synthesis, characterization and stability. Hydrometallurgy, 2017, 169, 263-274.	4.3	16
44	Light-assisted delithiation of lithium iron phosphate nanocrystals towards photo-rechargeable lithium ion batteries. Nature Communications, 2017, 8, 14643.	12.8	179
45	In Operando XANES & XRD Investigation into the Rate-Dependent Transport Properties of Lithium Iron Silicate Cathodes. MRS Advances, 2017, 2, 419-424.	0.9	1
46	Nanostructural and photo-electrochemical properties of solution spin-coated Cu ₂ ZnSnS ₄ –TiO ₂ nanorod forest films with an improved photovoltaic performance. Nanoscale, 2017, 9, 7650-7665.	5.6	14
47	A green process for recovery of H ₂ SO ₄ and Fe ₂ O ₃ from FeSO ₄ Â-7H ₂ O by modeling phase equilibrium of the Fe(ĐŸ)––H ⁺ –Cl [–] system. AICHE Journal, 2017, 63, 4549-4563.	3.6	14
48	Modeling of glycine solubility in aqueous HCl–MgCl 2 system and its application in phase transition of glycine by changing media and supersaturation. Journal of Crystal Growth, 2017, 467, 116-125.	1.5	11
49	Investigating arsenic speciation in the JEB Tailings Management Facility at McClean Lake, Saskatchewan using X-ray absorption spectroscopy. Chemical Geology, 2017, 466, 617-626.	3.3	10
50	Solubility of NaHCO ₃ and NH ₄ HCO ₃ in the Relevant Media and Prediction of High-Pressure Phase Equilibria for the NH ₃ –CO ₂ –NaCl–H ₂ O System. Journal of Chemical & Engineering Data, 2017, 62, 4401-4410.	1.9	7
51	Capacity Fade Mechanism of Li ₄ Ti ₅ O ₁₂ Nanosheet Anode. Advanced Energy Materials, 2017, 7, 1601825.	19.5	67
52	Electron Dose Management for High Angle Annular Dark Field Scanning Transmission Electron Microscope Tomography of Beam Sensitive Materials. Microscopy and Microanalysis, 2016, 22, 1294-1295.	0.4	0
53	Stability of arsenate-bearing Fe(III)/Al(III) co-precipitates in the presence of sulfide as reducing agent under anoxic conditions. Chemosphere, 2016, 151, 318-323.	8.2	16
54	Process for Glycine Production by Antisolvent Crystallization Using Its Phase Equilibria in the Ethylene Glycol–NH ₄ Cl–Water System. Industrial & Engineering Chemistry Research, 2016, 55, 2426-2437.	3.7	10

#	Article	IF	CITATIONS
55	Density functional theory insights into the structural stability and Li diffusion properties of monoclinic and orthorhombic Li 2 FeSiO 4 cathodes. Journal of Power Sources, 2016, 318, 136-145.	7.8	34
56	Nanoscale Photo-Absorbing Kesterite Grown on Anatase Mesoscopic Films by Sequential Binary Chalcogenide Solution Deposition-Exchange, Annealing, and Etching. Crystal Growth and Design, 2016, 16, 3618-3630.	3.0	9
57	Understanding the phase formation kinetics of nano-crystalline kesterite deposited on mesoscopic scaffolds via in situ multi-wavelength Raman-monitored annealing. Physical Chemistry Chemical Physics, 2016, 18, 29435-29446.	2.8	11
58	Steady‣tate, Scalable Production of Mesoporous Rutile and Brookite Particles and Their Use in Energy Conversion and Storage Cells. ChemNanoMat, 2016, 2, 980-988.	2.8	3
59	Li-ion storage dynamics in metastable nanostructured Li2FeSiO4 cathode: Antisite-induced phase transition and lattice oxygen participation. Journal of Power Sources, 2016, 329, 355-363.	7.8	26
60	Antimony in the metallurgical industry: A review of its chemistry and environmental stabilization options. Hydrometallurgy, 2016, 164, 141-153.	4.3	105
61	Transient existence of crystalline lithium disulfide Li2S2 in a lithium-sulfur battery. Journal of Power Sources, 2016, 325, 641-645.	7.8	57
62	Formation of Lithium Titanate Hydrate Nanosheets: Insight into a Two-Dimension Growth Mechanism by in Situ Raman. Crystal Growth and Design, 2016, 16, 3898-3904.	3.0	9
63	Stabilization of iron arsenate solids by encapsulation with aluminum hydroxyl gels. Journal of Chemical Technology and Biotechnology, 2016, 91, 408-415.	3.2	17
64	Continuous-reactor, pH-controlled synthesis of multifunctional mesoporous nanocrystalline anatase aggregates. Chemical Engineering Journal, 2016, 287, 398-409.	12.7	7
65	Aqueous, Screen-Printable Paste for Fabrication of Mesoporous Composite Anatase–Rutile TiO ₂ Nanoparticle Thin Films for (Photo)electrochemical Devices. ACS Sustainable Chemistry and Engineering, 2016, 4, 2173-2181.	6.7	22
66	Accelerated Removal of Fe-Antisite Defects while Nanosizing Hydrothermal LiFePO ₄ with Ca ²⁺ . Nano Letters, 2016, 16, 2692-2697.	9.1	52
67	Spontaneous reaction between an uncharged lithium iron silicate cathode and a LiPF ₆ -based electrolyte. Chemical Communications, 2016, 52, 190-193.	4.1	14
68	Investigation of sodium silicate-derived gels as encapsulants for hazardous materials – The case of scorodite. Journal of Hazardous Materials, 2015, 292, 108-117.	12.4	33
69	New Insight into the Atomic-Scale Bulk and Surface Structure Evolution of Li ₄ Ti ₅ O ₁₂ Anode. Journal of the American Chemical Society, 2015, 137, 1581-1586.	13.7	106
70	Oxidation of Ferrous Sulfate Hydrolyzed Slurry—Kinetic Aspects and Impact on As(V) Removal. Industrial & Engineering Chemistry Research, 2015, 54, 1738-1747.	3.7	6
71	Engineering 3-D Li-Ion Electrodes with Enhanced Charge Storage Properties Based on Solution-Processed and Sintered Anatase Nanocrystal-Carbon Mesoporous Structures. ACS Sustainable Chemistry and Engineering, 2015, 3, 334-339.	6.7	4
72	From extractive metallurgy to materials engineering: personal teaching and research perspective. Canadian Metallurgical Quarterly, 2015, 54, 129-135.	1.2	0

GEORGE P DEMOPOULOS

#	Article	IF	CITATIONS
73	Stability of continuously produced Fe(II)/Fe(III)/As(V) co-precipitates under periodic exposure to reducing agents. Chemosphere, 2015, 138, 239-246.	8.2	16
74	Cation exchange mediated elimination of the Fe-antisites in the hydrothermal synthesis of LiFePO4. Nano Energy, 2015, 16, 256-267.	16.0	54
75	Rate-dependent phase transitions in Li2FeSiO4 cathode nanocrystals. Scientific Reports, 2015, 5, 8599.	3.3	31
76	Water activity-based design of a single-stage CSTR reactive crystallization process for producing super-azeotropic HCl and well grown metastable 1±-calcium sulfate hemihydrate crystals from CaCl2 solution. Hydrometallurgy, 2015, 155, 20-28.	4.3	11
77	Growth of Cu ₂ ZnSnS ₄ Nanocrystallites on TiO ₂ Nanorod Arrays as Novel Extremely Thin Absorber Solar Cell Structure via the Successive-Ion-Layer-Adsorption-Reaction Method. ACS Applied Materials & amp; Interfaces, 2015, 7, 22888-22897.	8.0	39
78	Enabling Green Fabrication of Li-Ion Battery Electrodes by Electrophoretic Deposition: Growth of Thick Binder-Free Mesoporous TiO ₂ -Carbon Anode Films. Journal of the Electrochemical Society, 2015, 162, D3013-D3018.	2.9	19
79	Incorporation of arsenic into gypsum: Relevant to arsenic removal and immobilization process in hydrometallurgical industry. Journal of Hazardous Materials, 2015, 300, 272-280.	12.4	80
80	Anodized aluminum–silicon alloy counter electrode substrates for next generation solar cell applications. Applied Surface Science, 2015, 356, 317-324.	6.1	10
81	Continuous circuit coprecipitation of arsenic(V) with ferric iron by lime neutralization: The effect of circuit staging, co-ions and equilibration pH on long-term arsenic retention. Hydrometallurgy, 2015, 151, 42-50.	4.3	38
82	Organic solventâ€assisted crystallization of inorganic salts from acidic media. Journal of Chemical Technology and Biotechnology, 2015, 90, 686-692.	3.2	21
83	Spatial Distribution of Light Scattering and Absorption Interactions with TiO2- Nanoparticles from Monte Carlo and Generalized-Multiparticle-Mie based Simulations for Dye-Sensitized Solar Cell Analysis and Optimization. Microscopy and Microanalysis, 2014, 20, 548-549.	0.4	0
84	Effects of crystal habit modifiers on the morphology of calcium sulfate dihydrate grown in strong <scp>CaCl₂â€HCl</scp> solutions. Journal of Chemical Technology and Biotechnology, 2014, 89, 1523-1533.	3.2	31
85	Greenâ€Engineered Allâ€Substrate Mesoporous TiO ₂ Photoanodes with Superior Lightâ€Harvesting Structure and Performance. ChemSusChem, 2014, 7, 813-821.	6.8	17
86	Comparative molecular characterization of aluminum hydroxyâ€gels derived from chloride and sulphate salts. Journal of Chemical Technology and Biotechnology, 2014, 89, 206-213.	3.2	12
87	Stirring effect in hydrothermal synthesis of nano C-LiFePO4. Journal of Power Sources, 2014, 266, 99-106.	7.8	52
88	Development of Titanium-Sputtered Anodized Aluminum Substrates for Dye-Sensitized Solar Cells. Metallurgical and Materials Transactions E, 2014, 1, 311-317.	0.5	2
89	Phase Equilibria for the Glycine–Methanol–NH ₄ Cl–H ₂ O System. Industrial & Engineering Chemistry Research, 2014, 53, 16864-16872.	3.7	15
90	Direct imaging of layered O3- and P2-Na _x Fe _{1/2} Mn _{1/2} O ₂ structures at the atomic scale. Physical Chemistry Chemical Physics, 2014, 16, 21946-21952.	2.8	50

#	Article	IF	CITATIONS
91	Determination and Modeling of the Solubility of Na ₂ SiO ₃ ·9H ₂ O in the NaCl–KCl–H ₂ O System. Journal of Chemical & Engineering Data, 2014, 59, 1264-1272.	1.9	12
92	On the complex interplay of crystallinity and surface area effects on Li-ion intercalation and pseudocapacitive storage properties of nanocrystalline anatase. Journal of Power Sources, 2014, 272, 58-67.	7.8	15
93	Precipitation behaviour of As(V) during neutralization of acidic Fe(II)â^'As(V) solutions in batch and continuous modes. Hydrometallurgy, 2014, 146, 40-47.	4.3	36
94	Measurement and Chemical Modeling of the Solubility of Na ₂ SiO ₃ ·9H ₂ O and Na ₂ SiO ₃ in Concentrated NaOH Solution from 288 to 353 K. Industrial & Engineering Chemistry Research, 2014, 53, 9949-9958.	3.7	18
95	Mesoporous Brookite Nanoplatelets with Superior Lithium-ion Intercalation Stability. Electrochimica Acta, 2014, 138, 215-223.	5.2	9
96	Transmission Electron Forward Scattered Diffraction and Low Voltage SEM/STEM Characterization of Binder-Free TiO2 Electrodes. Microscopy and Microanalysis, 2014, 20, 492-493.	0.4	1
97	Electrophoretically self-assembled mixed metal oxide-TiO2 nano-composite film structures for photoelectrochemical energy conversion: Probing of charge recombination and electron transport resistances. Journal of Power Sources, 2013, 240, 667-675.	7.8	17
98	Aqueous Synthesized Nanostructured Li ₄ Ti ₅ O ₁₂ for High-Performance Lithium Ion Battery Anodes. Journal of the Electrochemical Society, 2013, 160, A3041-A3047.	2.9	19
99	Enabling aqueous electrophoretic growth of adherent nanotitania mesoporous films via intrafilm cathodic deposition of hydrous zinc oxide. Electrochimica Acta, 2013, 87, 169-179.	5.2	12
100	Size-Dependent Maximization of Upconversion Efficiency of Citrate-Stabilized β-phase NaYF ₄ :Yb ³⁺ ,Er ³⁺ Crystals via Annealing. ACS Applied Materials & Interfaces, 2013, 5, 11661-11667.	8.0	90
101	Annealing-induced ultra-efficient NIR-to-VIS upconversion of nano-/micro-scale α and β NaYF4:Er3+,Yb3+ crystals. CrystEngComm, 2013, 15, 4739.	2.6	38
102	Influence of Impurities on Crystallization Kinetics of Calcium Sulfate Dihydrate and Hemihydrate in Strong HCl-CaCl ₂ Solutions. Industrial & Engineering Chemistry Research, 2013, 52, 6540-6549.	3.7	67
103	Thin single screen-printed bifunctional titania layer photoanodes for high performing DSSCs via a novel hybrid paste formulation and process. Journal of Materials Research, 2013, 28, 480-487.	2.6	17
104	Novel Mesoporous Nanotitania/Carbon Composite Electrodes for Electrochemical Energy Storage. ECS Transactions, 2013, 50, 37-48.	0.5	2
105	Hydrochloric Acid Regeneration via Calcium Sulfate Crystallization for Non-Ferrous Chloride Leaching Processes. , 2013, , 379-389.		0
106	Continuous Co-Precipitation Behaviour and Stability of Arsenic(V) from Fe(II,III)-Al(III)-Ni(II) Sulphate Effluent Solutions. , 2013, , 371-378.		0
107	The Rapid Measurement and Monitoring of Selenite Concentration by Turbidimetry Following its Conversion to Colloidal State by Sulfite Reduction and Acidification. Separation Science and Technology, 2012, 47, 677-683.	2.5	0
108	A novel two-step coprecipitation process using Fe(III) and Al(III) for the removal and immobilization of arsenate from acidic aqueous solution. Water Research, 2012, 46, 500-508.	11.3	57

GEORGE P DEMOPOULOS

#	Article	IF	CITATIONS
109	Colloidal PbS and PbSeS Quantum Dot Sensitized Solar Cells Prepared by Electrophoretic Deposition. Journal of Physical Chemistry C, 2012, 116, 16391-16397.	3.1	81
110	The crystal growth kinetics of alpha calcium sulfate hemihydrate in concentrated CaCl2–HCl solutions. Journal of Crystal Growth, 2012, 351, 9-18.	1.5	50
111	Phase transformation kinetics of calcium sulfate phases in strong CaCl2HCl solutions. Hydrometallurgy, 2012, 129-130, 126-134.	4.3	32
112	Continuous circuit coprecipitation of arsenic(V) with ferric iron by lime neutralization: Process parameter effects on arsenic removal and precipitate quality. Hydrometallurgy, 2012, 111-112, 65-72.	4.3	88
113	Enhanced surface hydroxylation of nanocrystalline anatase films improves photocurrent output and electron lifetime in dye sensitized solar cell photoanodes. Electrochimica Acta, 2012, 67, 208-215.	5.2	32
114	Stannous chloride—an effective reducing agent for the removal of selenium(IV) from acidic solution. Journal of Chemical Technology and Biotechnology, 2012, 87, 983-989.	3.2	4
115	Further Understanding of the Electronic Interactions between N719 Sensitizer and Anatase TiO ₂ Films: A Combined X-ray Absorption and X-ray Photoelectron Spectroscopic Study. Journal of Physical Chemistry C, 2011, 115, 5692-5707.	3.1	72
116	Enhanced Performance of Dye-Sensitized Solar Cells by Utilization of an External, Bifunctional Layer Consisting of Uniform β-NaYF ₄ :Er ³⁺ /Yb ³⁺ Nanoplatelets. ACS Applied Materials & Interfaces, 2011, 3, 3239-3243.	8.0	126
117	The effect of copper on the precipitation of scorodite (FeAsO4·2H2O) under hydrothermal conditions: Evidence for a hydrated copper containing ferric arsenate sulfate-short lived intermediate. Journal of Colloid and Interface Science, 2011, 360, 508-518.	9.4	34
118	Raman spectroscopic study of the hydrogen and arsenate bonding environment in isostructural synthetic arsenates of the variscite group—M ³⁺ AsO ₄ ·2H ₂ O (M ³⁺ = Fe, Al, In and Ga): implications for arsenic release in water. Journal of Raman Spectroscopy, 2011, 42, 62-71.	2.5	14
119	Hydrothermal reaction chemistry and characterization of ferric arsenate phases precipitated from Fe2(SO4)3–As2O5–H2SO4 solutions. Hydrometallurgy, 2011, 107, 74-90.	4.3	80
120	The elimination of selenium(IV) from aqueous solution by precipitation with sodium sulfide. Journal of Hazardous Materials, 2011, 185, 148-154.	12.4	73
121	Preparation of DSSC Nanotitania Thin Film Photoanodes by Electrophoretic Deposition in an Aqueous Suspension. ECS Transactions, 2011, 35, 39-52.	0.5	1
122	Vibrational spectroscopy study of hydrothermally produced scorodite (FeAsO ₄ ·2H ₂ O), ferric arsenate subâ€hydrate (FAsH;) Tj ETQq0 0 0 rgBT /Overlock 10	Tf 50 227 2.5	Td (FeAsO< 24
123	Journal of Raman Spectroscopy, 2010, 41, 212-221. Nearâ€Infrared Sunlight Harvesting in Dyeâ€&ensitized Solar Cells Via the Insertion of an Upconverterâ€TiO ₂ Nanocomposite Layer. Advanced Materials, 2010, 22, 4373-4377.	21.0	291
124	Scorodite encapsulation by controlled deposition of aluminum phosphate coatings. Journal of Hazardous Materials, 2010, 181, 526-534.	12.4	39
125	Raman Spectroscopy in the Hydrometallurgical and Materials Engineering World. , 2010, , .		0
126	The synthesis of aqueous-dispersible anatase TiO ₂ nanoplatelets. Nanotechnology, 2010, 21, 025604.	2.6	42

#	Article	IF	CITATIONS
127	Molecular and structural investigation of yukonite (synthetic & natural) and its relation to arseniosiderite. Geochimica Et Cosmochimica Acta, 2010, 74, 5835-5851.	3.9	35
128	Further Understanding of the Adsorption Mechanism of N719 Sensitizer on Anatase TiO ₂ Films for DSSC Applications Using Vibrational Spectroscopy and Confocal Raman Imaging. Langmuir, 2010, 26, 9575-9583.	3.5	202
129	Effects of Temperature on the Preparation of Magnesium Carbonate Hydrates by Reaction of MgCl2 with Na2CO3. Chinese Journal of Chemical Engineering, 2009, 17, 661-666.	3.5	38
130	Nucleation and growth of self-assembled nanofibre-structured rutile (TiO2) particles via controlled forced hydrolysis of titanium tetrachloride solution. Journal of Crystal Growth, 2009, 312, 86-94.	1.5	35
131	Nanocrystalline TiO2 thin film electrodes for dye-sensitized solar cell applications. Jom, 2009, 61, 52-57.	1.9	18
132	Gypsum crystallization and hydrochloric acid regeneration by reaction of calcium chloride solution with sulfuric acid. Hydrometallurgy, 2009, 96, 95-102.	4.3	40
133	Aqueous precipitation and crystallization for the production of particulate solids with desired properties. Hydrometallurgy, 2009, 96, 199-214.	4.3	128
134	The dissolution of scorodite in gypsum-saturated waters: Evidence of Ca–Fe–AsO4 mineral formation and its impact on arsenic retention. Hydrometallurgy, 2009, 97, 221-227.	4.3	47
135	Desilication of sodium aluminate solution by Friedel's salt (FS: 3CaO·A12O3·CaCl2·10H2O). Hydrometallurgy, 2009, 99, 225-230.	4.3	37
136	Solubility and Stability of Nesquehonite (MgCO ₃ ·3H ₂ O) in Mixed NaCl + MgCl ₂ , NH ₄ Cl + MgCl ₂ , LiCl, and LiCl + MgCl ₂ Solutions. Journal of Chemical & Engineering Data, 2009, 54, 3002-3007.	1.9	17
137	Structural characterization of poorly-crystalline scorodite, iron(III)–arsenate co-precipitates and uranium mill neutralized raffinate solids using X-ray absorption fine structure spectroscopy. Geochimica Et Cosmochimica Acta, 2009, 73, 3260-3276.	3.9	79
138	Synthesis of Hydroxyl-Rich Anatase Nanocrystallites, Their Characterization and Performance as Photoanode in Dye-Sensitized Solar Cells. ECS Transactions, 2009, 21, 23-34.	0.5	12
139	Reductive Precipitation of Elemental Selenium from Selenious Acidic Solutions Using Sodium Dithionite. Industrial & Engineering Chemistry Research, 2009, 48, 10240-10246.	3.7	44
140	Controlled precipitation of nesquehonite (MgCO3·3H2O) by the reaction of MgCl2 with (NH4)2CO3. Journal of Crystal Growth, 2008, 310, 1220-1227.	1.5	82
141	Precipitation of nanosized titanium dioxide from aqueous titanium(IV) chloride solutions by neutralization with MgO. Hydrometallurgy, 2008, 90, 26-33.	4.3	28
142	Coprecipitation of arsenate with iron(III) in aqueous sulfate media: Effect of time, lime as base and co-ions on arsenic retention. Water Research, 2008, 42, 661-668.	11.3	140
143	Solubility and Stability of Nesquehonite (MgCO ₃ ·3H ₂ O) in NaCl, KCl, MgCl ₂ , and NH ₄ Cl Solutions. Journal of Chemical & Engineering Data, 2008, 53, 2586-2593.	1.9	39
144	Infrared spectroscopic and X-ray diffraction characterization of the nature of adsorbed arsenate on ferrihydrite. Geochimica Et Cosmochimica Acta, 2007, 71, 1643-1654.	3.9	282

GEORGE P DEMOPOULOS

#	Article	IF	CITATIONS
145	Synthesis, Structure, and Stability of Gallium Arsenate Dihydrate, Indium Arsenate Dihydrate, and Lanthanum Arsenate. Industrial & Engineering Chemistry Research, 2007, 46, 7875-7882.	3.7	12
146	Speciation-Based Chemical Equilibrium Model of CaSO4Solubility in the H + Na + Ca+ Mg + Al + Fe(II) + Cl + SO4+ H2O System. Industrial & Engineering Chemistry Research, 2007, 46, 6385-6392.	3.7	13
147	The incongruent dissolution of scorodite — Solubility, kinetics and mechanism. Hydrometallurgy, 2007, 87, 163-177.	4.3	130
148	Gas transfer kinetics and redox potential considerations in oxidative precipitation of manganese from an industrial zinc sulphate solution with SO2/O2. Hydrometallurgy, 2007, 89, 357-368.	4.3	14
149	Hydrothermal Synthesis and Stability Evaluation of Iron (III)-Aluminum (III) Arsenate Solid Solutions. Metallurgical and Materials Transactions B: Process Metallurgy and Materials Processing Science, 2007, 38, 159-166.	2.1	17
150	Characterization of Poorly-Crystalline Ferric Arsenate Precipitated from Equimolar Fe(III)-As(V) Solutions in the pH Range 2 to 8. Metallurgical and Materials Transactions B: Process Metallurgy and Materials Processing Science, 2007, 38, 751-762.	2.1	47
151	Observation of Surface Precipitation of Arsenate on Ferrihydrite. Environmental Science & Technology, 2006, 40, 3248-3253.	10.0	245
152	Model-Based Construction of Calcium Sulfate Phase-Transition Diagrams in the HClâ^'CaCl2â^'H2O System between 0 and 100 °C. Industrial & Engineering Chemistry Research, 2006, 45, 4517-4524.	3.7	76
153	Development of an Improved Chemical Model for the Estimation of CaSO4Solubilities in the HClâ^'CaCl2â^'H2O System up to 100 °C. Industrial & Engineering Chemistry Research, 2006, 45, 2914-2922.	3.7	35
154	Effect of NaCl, MgCl2, FeCl2, FeCl3, and AlCl3on Solubility of CaSO4Phases in Aqueous HCl or HCl + CaCl2Solutions at 298 to 353 K. Journal of Chemical & Engineering Data, 2006, 51, 569-576.	1.9	28
155	Acidity, valency and third-ion effects on the precipitation of scorodite from mixed sulfate solutions under atmospheric-pressure conditions. Metallurgical and Materials Transactions B: Process Metallurgy and Materials Processing Science, 2006, 37, 189-197.	2.1	70
156	Comparative study of iron(III) separation from zinc sulphate–sulphuric acid solutions using organophosphorus extractants, OPAP and D2EHPA. Hydrometallurgy, 2005, 79, 97-109.	4.3	27
157	Temperature and seeding effects on the precipitation of scorodite from sulfate solutions under atmospheric-pressure conditions. Metallurgical and Materials Transactions B: Process Metallurgy and Materials Processing Science, 2005, 36, 327-333.	2.1	88
158	Solubility of CaSO4 Phases in Aqueous HCl + CaCl2 Solutions from 283 K to 353 K. Journal of Chemical & Engineering Data, 2005, 50, 1971-1982.	1.9	84
159	Preparation of α-Calcium Sulfate Hemihydrate by Reaction of Sulfuric Acid with Lime. Industrial & Engineering Chemistry Research, 2005, 44, 715-724.	3.7	52
160	Synthesis of Hydrated Aluminum Phosphate, AlPO4·1.5H2O (AlPO4â^'H3), by Controlled Reactive Crystallization in Sulfate Media. Industrial & Engineering Chemistry Research, 2005, 44, 8033-8038.	3.7	23
161	Adsorption of Arsenate onto Ferrihydrite from Aqueous Solution:Â Influence of Media (Sulfate vs) Tj ETQq1 1 0.7 9523-9527.	84314 rgB 10.0	T /Overlock 136
162	Stripping of Rh–Sn–Cl-loaded alkylated 8-hydroxyquiniline with Na2SO3–HCl. Journal of Chemical Technology and Biotechnology, 2004, 79, 187-194.	3.2	0

#	Article	IF	CITATIONS
163	Comparative study of iron(III) separation from zinc sulphate–sulphuric acid solutions using the organophosphorus extractants, OPAP and D2EHPA. Hydrometallurgy, 2004, 74, 93-102.	4.3	37
164	Solubility of Calcium Sulfate Hydrates in (0 to 3.5) mol·kg-1Sulfuric Acid Solutions at 100 °C. Journal of Chemical & Engineering Data, 2004, 49, 1263-1268.	1.9	35
165	Hydrolysis of Ferric Sulfate in the Presence of Zinc Sulfate at 200 °C: Precipitation Kinetics and Product Characterization. Industrial & Engineering Chemistry Research, 2004, 43, 6299-6308.	3.7	31
166	Nickel hydroxide precipitation from aqueous sulfate media. Jom, 2003, 55, 42-46.	1.9	28
167	The solubility and stability of organophosphoric acid extractants in H2SO4 and HCl media. Hydrometallurgy, 2003, 68, 115-124.	4.3	27
168	Adsorption of Silver onto Activated Carbon from Acidic Media:  Nitrate and Sulfate Media. Industrial & Engineering Chemistry Research, 2003, 42, 72-79.	3.7	35
169	Producing high-grade nickel sulfate with solvent displacement crystallization. Jom, 2002, 54, 49-53.	1.9	21
170	The kinetics of cobalt removal by cementation from an industrial zinc electrolyte in the presence of Cu, Cd, Pb, Sb and Sn additives. Hydrometallurgy, 2001, 60, 105-116.	4.3	38
171	A contribution to the measurement of oxygen mass transfer in a laboratory pressure reactor. Journal of Chemical Technology and Biotechnology, 2000, 75, 665-672.	3.2	5
172	Gas-Liquid Oxygen Mass-transfer; from Fundamentals to Applications in Hydrometallurgical Systems. Mineral Processing and Extractive Metallurgy Review, 2000, 20, 447-502.	5.0	0
173	Gas–Liquid Oxygen Mass-transfer; from Fundamentals to Applications in Hydrometallurgical Systems. Mineral Processing and Extractive Metallurgy Review, 2000, 20, 447-502.	5.0	3
174	Parameter sensitivity of kineticsâ€based hydrometallurgical reactor models. Canadian Journal of Chemical Engineering, 1998, 76, 1083-1092.	1.7	3
175	Formation and extraction of Rh-Sn-Cl complexes with an alkylated 8-hydroxyquinoline. Journal of Chemical Technology and Biotechnology, 1998, 72, 183-189.	3.2	11
176	Permeation of Iridium(IV) and Metal Impurity Chlorocomplexes through a Supported Liquid Membrane Designed for Rhodium Separation. Separation Science and Technology, 1998, 33, 1145-1162.	2.5	7
177	Optimizing Cu removal/recovery in a biosorption column. Water Research, 1997, 31, 2327-2339.	11.3	103
178	A kinetic study on the acid pressure leaching of pyrrhotite. Hydrometallurgy, 1997, 47, 1-18.	4.3	28
179	Steady-state modeling of zinc-ferrite hot-acid leaching. Metallurgical and Materials Transactions B: Process Metallurgy and Materials Processing Science, 1997, 28, 701-711.	2.1	14
180	Arsenic immobilization by controlled scorodite precipitation. Jom, 1997, 49, 52-55.	1.9	105

#	Article	IF	CITATIONS
181	Extraction of Rhodium Chlorocomplexes and Acid through a Supported Liquid Membrane of Kelex 100. Separation Science and Technology, 1996, 31, 895-914.	2.5	10
182	Extraction and Separation of HCl and Rh(III) with Trioctylamine. Journal of Chemical Technology and Biotechnology, 1996, 67, 367-375.	3.2	12
183	Speciation and separation of rhodium (III) from chloride solutions: a critical review. Hydrometallurgy, 1996, 40, 135-152.	4.3	176
184	Extraction and separation of HCl and Rh(III) with trioctylamine. , 1996, 67, 367.		1
185	Hydrogen ion activities and species distribution in mixed metal sulfate aqueous systems. AICHE Journal, 1995, 41, 171-184.	3.6	39
186	Formation of W/O Microemulsions in the Extraction System Rh(III)-HCl-Kelex 100 and Its Impact on Rh(III) Distribution. Journal of Colloid and Interface Science, 1995, 173, 448-459.	9.4	30
187	Precipitation of crystalline scorodite (FeAsO4 · 2H2O) from chloride solutions. Hydrometallurgy, 1995, 38, 245-261.	4.3	106
188	Assessment of alternative iron sources in the pressure leaching of zinc concentrates using a reactor model. Hydrometallurgy, 1995, 39, 147-162.	4.3	12
189	Mathematical modeling of the zinc pressure leach process. Metallurgical and Materials Transactions B: Process Metallurgy and Materials Processing Science, 1995, 26, 1035-1047.	2.1	30
190	NEW 8-HYDROXYQUINOLINE DERIVATIVE EXTRACTANTS FOR PLATINUM GROUP METALS SEPARATION PART 4: KINETICS OF Pd(II) EXTRACTION AND STRIPPING. Solvent Extraction and Ion Exchange, 1995, 13, 83-107.	2.0	9
191	AN INVESTIGATION ON THE EXTRACTION OF RHODIUM FROM AQUEOUS CHLORIDE SOLUTIONS WITH 7-SUBSTITUTED 8-HYDROXYQUINOLINES. Solvent Extraction and Ion Exchange, 1994, 12, 497-516.	2.0	41
192	NEW 8-HYDROXYQUINOLINE DERIVATIVE EXTRACTANTS FOR PLATINUM GROUP METALS SEPARATION PART 2: Pd(II) EXTRACTION EQUILIBRIA AND STRIPPING Solvent Extraction and Ion Exchange, 1994, 12, 393-421.	2.0	25
193	NEW 8-HYDROXYQUINOLINE DERIVATIVE EXTRACT ANTS FOR PLATINUM GROUP METALS SEPARATION PART 3: Pt(IV) EXTRACTION EQUILIBRIA AND STRIPPING. Solvent Extraction and Ion Exchange, 1994, 12, 517-540.	2.0	15
194	On the variable dissolution kinetics of zinc ferrite in acid media. Canadian Journal of Chemical Engineering, 1993, 71, 790-801.	1.7	13
195	NEW 8-HYDROXYQUINOUNE DERIVATIVE EXTRACTANTS FOR PLATINUM GROUP METAL SEPARATION PART 1: CHARACTERIZATION AND HCI XTRACTION. Solvent Extraction and Ion Exchange, 1993, 11, 349-376.	2.0	14
196	A Reaction Kinetic Model for the Leaching of Industrial Zinc Ferrite Particulates in Sulphuric Acid Media. Canadian Metallurgical Quarterly, 1992, 31, 41-54.	1.2	37
197	A Reaction Kinetic Model for the Leaching of Industrial Zinc Ferrite Particulates in Sulphuric Acid Media. Canadian Metallurgical Quarterly, 1992, 31, 41-54.	1.2	3
198	Acid pressure oxidation of pyrite: reaction kinetics. Hydrometallurgy, 1991, 26, 309-325.	4.3	55

#	Article	IF	CITATIONS
199	Mathematical modeling of an exothermic leaching reaction system: pressure oxidation of wide size arsenopyrite participates. Metallurgical and Materials Transactions B - Process Metallurgy and Materials Processing Science, 1990, 21, 827-837.	0.4	21
200	Acid Pressure Oxidation of Arsenopyrite: Part II, Reaction Kinetics. Canadian Metallurgical Quarterly, 1990, 29, 13-20.	1.2	35
201	Solvent Extraction of Iron(III) from Acid Sulphate Solutions by Mono(2-Ethyl Hexyl) Phosphoric Acid. Canadian Metallurgical Quarterly, 1989, 28, 13-18.	1.2	21
202	Iron(III) removal from base-metal electrolyte solutions by solvent extraction. Hydrometallurgy, 1984, 12, 299-315.	4.3	49
203	On the structure and composition of Kelex 100. Hydrometallurgy, 1983, 11, 389-396.	4.3	33
204	A study of the hydrogenation of kelex 100 loaded with copper. Journal of Chemical Technology and Biotechnology, Chemical Technology, 1983, 33, 249-260.	0.0	5